Modern methods for investigating the stability of a pitching floating platform wind turbine

Matthew Lennie[1], David Marten[1], George Pechlivanoglou[1], Christian Navid Nayeri[1], and Christian Oliver Paschereit[1]

Chair of Fluid Dynamics– Hermann-Föttinger-Institut – Technische Universität Berlin Müller-Breslau-Str. 8, 10623 Berlin Germany

Correspondence to: matthew.lennie@tu-berlin.de

Abstract. The QBlade implementation of the Lifting Line Free Vortex Wake method(LLFVW) was tested in conditions analogous to floating platform motion. Comparisons against two independent test cases, using a variety of simulation methods show excellent agreement in thrust forces, rotor power, blade forces and rotor plane induction. Along with the many verifications already undertaken in literature, it seems that the code performs solidly even in these challenging cases. Further to this, the key steps are presented from a new formulation of the instantaneous aerodynamic thrust damping of a wind turbine rotor. A test case with harmonic platform motion and collective pitch is used to demonstrate how combining such tools can lead to better understanding of aeroelastic stability.

1 Introduction

The proliferation of large wind turbine rotors has been accompanied by the need for accurate and computationally inexpensive aeroelastic simulation tools. For aeroelastic simulations, the aerodynamics of the wind turbine are most typically calculated using Blade Element Momentum based methods (BEM). In the scenario of offshore wind, particularly when designing for floating platforms, the significant motion of the rotor leads to complicated aerodynamics. Sebastian and Lackner (2013) have made a convincing case that, even with secondary correction factors, floating platform wind turbine aerodynamics exceed the capabilities of BEM based simulation methods. A prime example of this is concerning cases of rotor - wake interaction. As the rotor transitions between wind mill and propeller states, a toroidal recirculation pattern can form, meaning essentially that the rotor is interacting significantly with its own wake. As BEM does not explicitly solve the flow pattern of the wake, it is simply not possible to accurately represent such behaviour.

The Lifting Line Free Vortex Wake method (LLFVW) uses non-linear polar data to calculate the blade forces coupled with a free vortex wake formulation and serves as a good method for simulating cases where large rotor displacements and yaw misalignments occur (see figure 2). Recently, an implementation of a LLFVW code was completed and included in the QBlade wind turbine simulation code (Marten (2015)). Simultaneously to this study, the LLFVW solver is being extended to include an unsteady aerodynamics model and is being coupled with the structural formulations of the FAST framework (Wendler et al. (2016); Saverin et al. (2016)). In this paper, a comparison is made between the LLFVW code and existing literature comparisons where higher order aerodynamic simulation techniques were used i.e. URANS CFD (Tran et al. (2014); Sebastian

1

and Lackner (2013)). The comparisons and further test cases are made using the NREL 5MW reference turbine which is undergoing prescribed harmonic motion (see figure 1)(Jonkman (2013)).

After the validation of the LLFVW code for simulations involving a moving rotor plane, the aerodynamic damping of the rotor is investigated. For this analysis, a new formulation is presented for the instantaneous aerodynamic damping of the fore-aft motion degree of freedom. The formulation is a modification of an existing formulation that was first presented by Corke and Bowles (Bowles et al. (2014); Corke et al. (2014)) and later applied by Lennie to an airfoil with microtabs (Lennie et al. (2016)). For the first time, this new formulation makes it possible to look at the aerodynamic damping throughout the pitch cycle of the wind turbine - as opposed to the traditional approach where only cycled averaged values are inspected. Such a formulation is particularly useful for analysing aeroelastic instabilities where limit cycle oscillations are present. Limit cycle oscillations will have cycle averaged values that are neutral but could have occurrences of highly negative damping. Using this method on LLFVW data makes it possible to understand aeroelastic thrust stability of the rotor without the heavy linearisation applied in most stability analysis techniques. It is also a useful way of understanding the full effects of controller wind turbine interactions. An example will be presented showing the effect of collective pitch cycles during fore-aft motion of the rotor.

2 Rotor Motion

For the scope of this paper, prescribed motion of two varieties are considered. The first variety, pitching, is the more realistic representation where the rotor plane undergoes both pitch and linear translation (see figure 1). The second variety, fore-aft motion, assumes that the rotor plane pitching component is insignificant compared to the influence of the linear translation. Within the scope of this study, investigating the total rotor thrust, the difference between the assumptions is assumed to be small. There may be applications where this assumption is unsuitable. In the comparisons, the same magnitude and type of motion is used as in the literature so that no additional assumptions were introduced.

3 Comparison Cases

The QBlade LLFVW implementation has been previously tested for a range of standard HAWT and VAWT cases as can be found in existing literature (Marten (2015); Saverin et al. (2016)). When the wind turbine starts moving relative to the steady inflow, the wake will become distorted. In the case of a harmonic movement, the wake will display harmonic contractions and expansions (see figure 2) which induces velocity onto the rotor plane. The publications mentioned above have focused on verifying the performance of the QBlade LLFVW under stationary conditions and cases with yaw. This means that the battery of verifications undertaken should be extended to include cases where platform motion is present, thus ensuring that LLFVW techniques are a suitable approach for floating platform wind turbine aerodynamics. A number of comparison papers have been sought from literature that test a horizontal axis wind turbine rotor in prescribed floating platform motion. For the scope of this paper, only rigid body motion will be considered. The comparison will be undertaken by replicating the simulations from literature which used higher order methods.
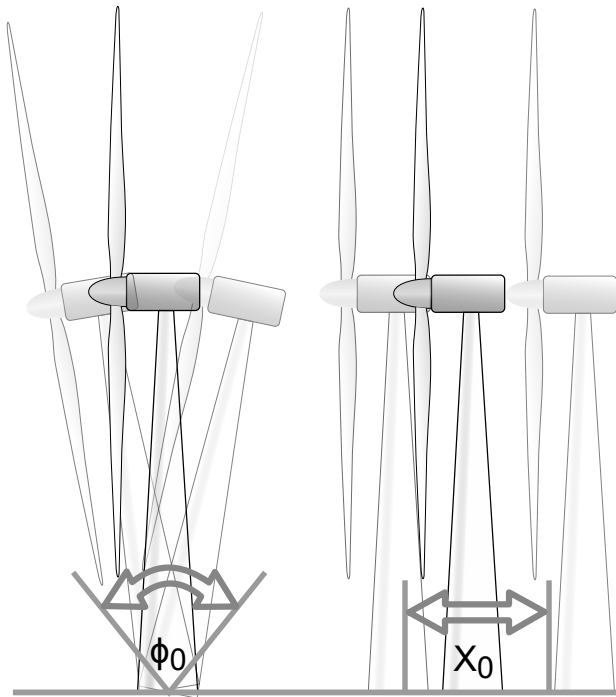
Figure 1. The two different assumed motions for the wind turbine. (Left: wind turbine pitching; Right: wind turbine fore-aft motion)
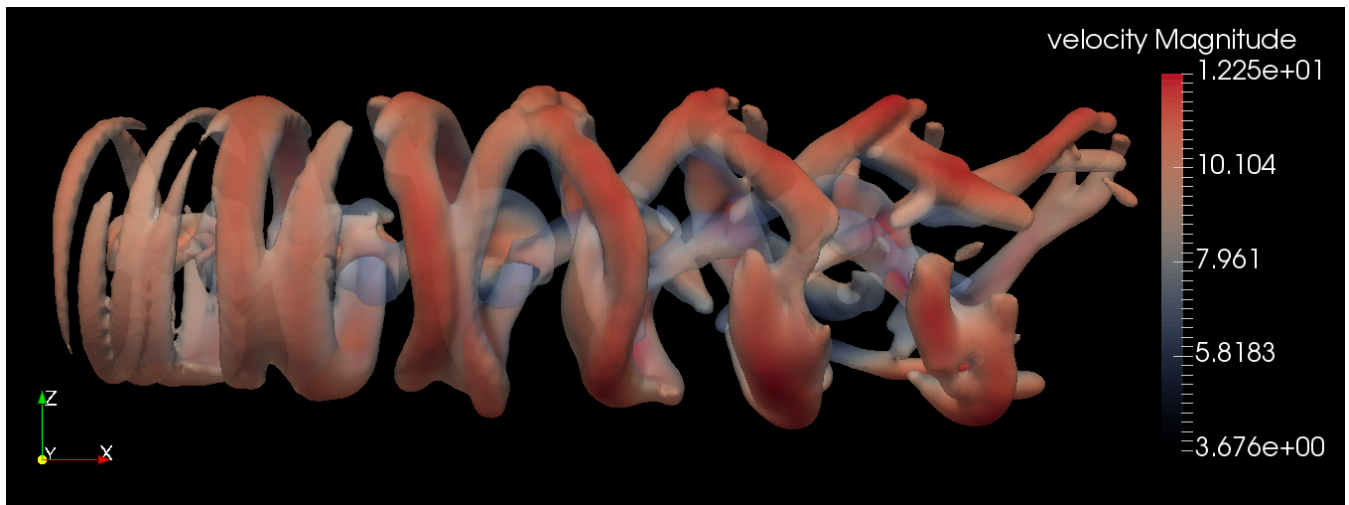

Figure 2. Snapshot of LLFVW simulation during pitching platform motion; vorticity isosurface of the wake coloured with velocity magnitude

Two different papers were used as a basis for comparison; both investigating the NREL 5MW reference turbine (Jonkman (2013)). Tran et al. (2014) compares a number of techniques with virtual blade motion using multiple reference frames (CFD-MRF) and real rigid body blade motion (CFD-RBM). The highest order simulation is a 3D Unsteady Reynolds Averaged Navier Stokes (URANS) CFD simulation with a $k-\omega$ shear-stress transport turbulence model. The blade rigid body motion was achieved using an over-set grid which is described at length including a discussion of the mesh convergence. The actual CFD simulations were conducted using commercial codes Fluent^{TM} with StarCCM+^{TM} for meshing. It appears from the presented information that the simulations should be high quality, within the limitations of URANS.

Tran et al. (2014) also compared their results against lower order simulations using unsteady blade element momentum method. The Tran et al. (2014) implementation of the unsteady blade element moment method (UBEM) was taken from Hansen (2008) with corrections for tip losses, wake unsteadiness and unsteady aerodynamics. This particular implementation took the platform motion into account by changing the relative inflow velocity. Further comparisons were made using modified versions of FAST(Jonkman (2013)) from the National Renewable Energy Laboratory; one comparison using a momentum balance for the wake solution (FAST-BEM) and the other using generalized dynamic wake (FAST-GDW). In both cases, the structural modes were locked and no controller was used, for more complete details, see the original paper from Tran et al. (2014).

Tran et al. (2014) simulates the pitching of the wind turbine as shown in figure 1(see left hand side). Two cases were simulated with platform pitching amplitudes of $1°$ and $4°$; and a constant harmonic pitching frequency of 0.1Hz. The calculations were performed at a steady inflow speed of 11m/s with a constant rotational speed of 12rpm and a constant blade pitch angle of $0°$. From this paper it was possible to compare thrust, power and integrated blade forces.
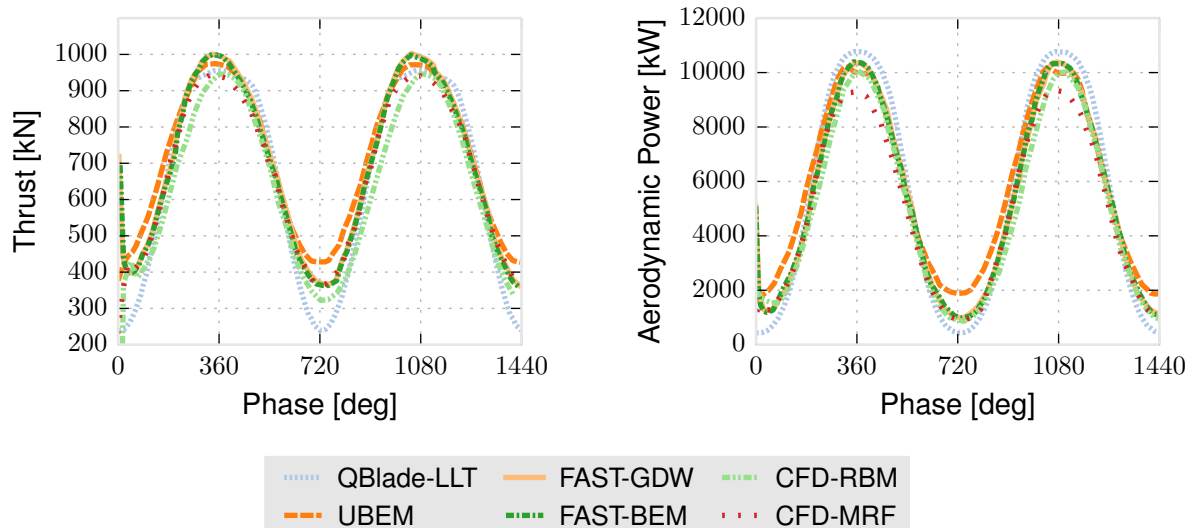
Figure 3. Thrust and power over phase angle for pitching platform motion ($4°$ pitch amplitude) Comparison Case: Tran et al. (2014)
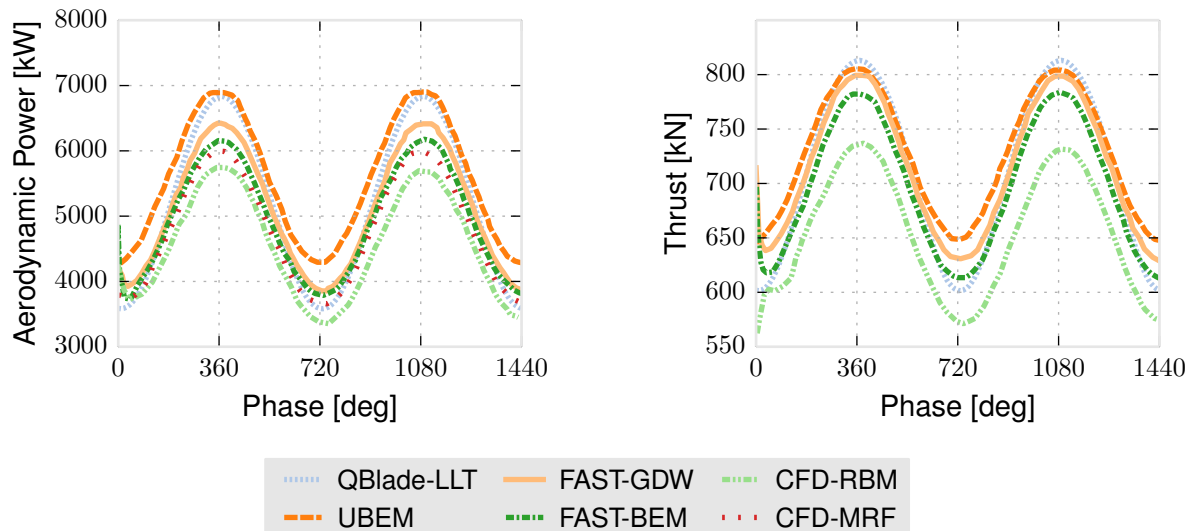
Figure 4. Thrust and power over phase angle for pitching platform motion ($1°$ pitch amplitude) Comparison Case: Tran et al. (2014)
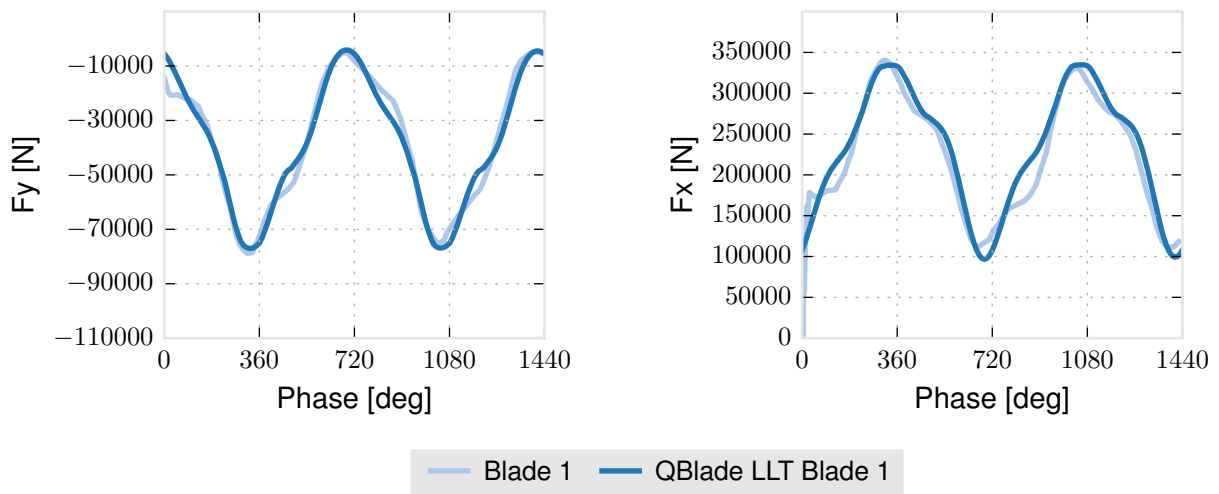
Figure 5. Integrated blade forces at blade root for pitching platform motion ($4°$ pitch amplitude) Comparison Case: Tran et al. (2014)

The QBlade simulations were run with the same conditions as described above. The unsteady aerodynamic model from Wendler was enabled without vortex lift as the wind turbine is operating at near rated speed without yaw(Wendler et al. (2016)). The standard NREL 5MW model (Jonkman (2013)) was set-up according to the definition[1]. The following settings were used for the simulation;

---

[1]The standard 5MW project file is available for download with the standard QBlade package
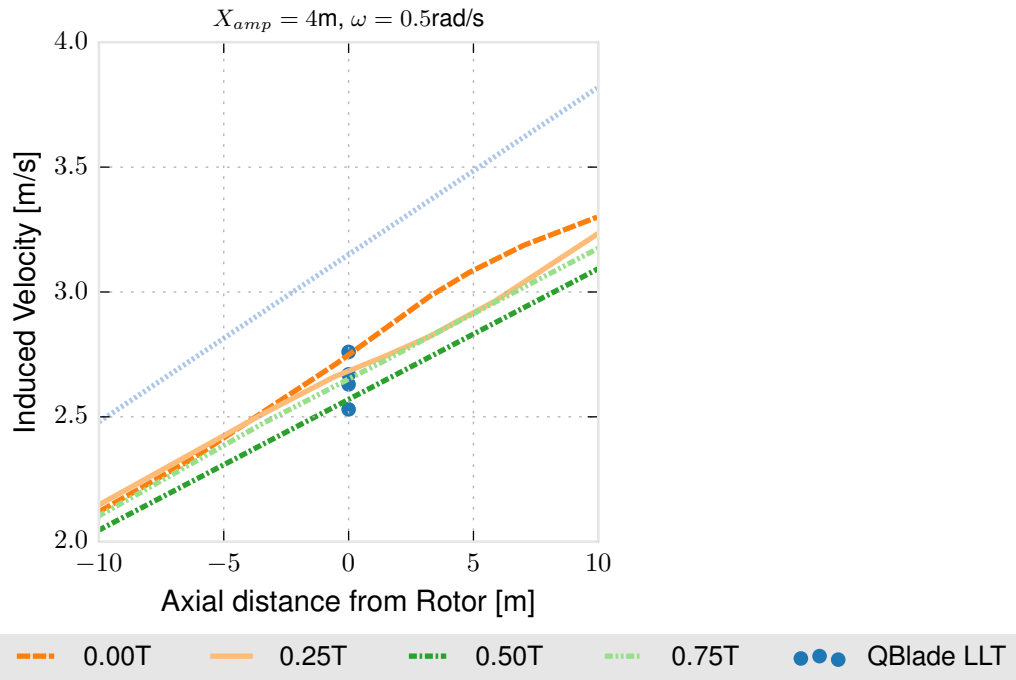
Figure 6. Induction Plot compared to Moving Actuator Disc CFD Hybrid from Vaal et al. (2014)

Wake Age in Revolutions	8
Full Wake in Revolutions	0.5
Fine Wake in Revolutions	4
Wake Thin Factor	2
Min Gamma Factor	0.4
First Row Length Fraction	0.3
Bound Vortex Location	0.4% c
Timestep	0.1 Sec

The LLFVW (figure 2) shows moderately good agreement for all cases, which can be seen in figures 3, 4 and 5. It is interesting to note that steady and even unsteady BEM simulations, when compared to CFD or LLFVW results, under predict the magnitude of the load cycle in most cases. The three classes of simulations compared all face limitations. The LLFVW and BEM cases both rely on 2D polar data which is sensitive to measurement or simulation settings like wind tunnel turbulence or turbulence model. Lennie et al. (2015) and Eisele et al. (2013) have shown that quality of the 2D polar data is crtical for power and loads prediction. For the BEM based methods, it is expected that the empirical corrections will struggle to represent the complicated fore-aft motion. The CFD solutions are based Un-steady Reynolds Averaged Navier(URANS) stokes equations.

After conducting thorough verification and validations of multiple URANs solvers with multiple turbulence closure models, Rumsey showed that URANS based models have a very limited ability to model cases with separation (Stangfeld et al. (2015) and Christopher L. Rumsey (2016)). Furthermore, the tendency of URANS codes to smear vorticity will cause errors in the wake induction in the cases where the blades are modeled. With each of the simulation methods facing some sort of limitation, it is difficult to choose one method as the baseline or "most" accurate. Nonetheless, integrated blade forces agree well for the CFD from Tran et al. (2014) and the LLFVW (see figure 5). Discrepancies in thrust and power can be seen in figures 3 and 4, but they are of a reasonable magnitude.

In the publication chosen for a second comparison, Vaal et al. (2014) uses a moving actuator disc CFD hybrid method which allows for a good comparison of the unsteady wake induction between CFD and the LLFVW. The moving actuator disk model essentially places a moveable actuator disk into a CFD simulation (Implemented in Fluent^{TM}). In practice this means that the actuator disk acts as a volume force onto the surrounding cells. It is argued by Vaal et al. (2014) that, because this method explicitly solves the wake rather than relying on simplified relations, the method should be more robust than the commonly used methods such as the Pit-Peters model (Pitt and Peters (1983)) or the Stig-Oye model(Hansen (2008)). Vaal et al. (2014) presents a number of investigations into the relative performance of the models, for this paper, the rotor plane induction is the most interesting to compare.

Vaal et al. (2014) undertook a sensitivity study showing the wake velocity before and after the rotor at different phases for different operating conditions. From this study, the authors choose the largest amplitude (16m) of fore-aft movement (right hand side of figure 1). The fore-aft motion was harmonic with a frequency of $0.08Hz$, the inflow speed was 11.2m/s, the blade pitch was $0°$ and the rotor speed was a constant $0.2Hz$. Vaal et al. (2014) allowed several oscillations to pass in order to let the wake effects develop. The grid extended 10 rotor diameters up and down stream. It would appear that the approach and settings used by Vaal et al. (2014) will provide good quality results for comparison.

The QBlade simulations were conducted again, using the settings stated above, with prescribed linear rotor plane movement. Like Vaal et al. (2014), a number of oscillations were simulated before finally extracting the data. The comparison was made at the exact rotor plane where the axial velocity could be sampled over an area determined by the rotor radius. There was not enough information provided by Vaal et al. (2014) to ensure consistency of the sampling area for the induced velocity. In the context of a wake with expansion and contraction occurring, the assumptions have a distinct effect on the induction results. Therefore, no upstream or downstream comparisons were attempted. A rotor plane axial velocity field snapshot was taken at equally spaced points within the cycle. The results, shown in figure 6, show that the rotor plane induction for the two methods matches well over the four snapshots. It seems therefore that there is a good agreement between the two methods for the most challenging test case presented by Vaal et al. (2014).

From the two verifications performed here it seems that the QBlade LLFVW simulation model produces results that are comparable to other higher order or hybrid methods. These results and the results already published give a high degree of confidence in the simulation tools ability to model wind turbines undergoing platform motion.

4 Using the Hilbert Transform method to obtain instantaneous aerodynamic damping of a pitching rotor

The following section briefly outlines a reformulation of the instantaneous damping calculation method outlined by Bowles and Corke (Bowles et al. (2014); Corke et al. (2014)). The original reference by Bowles et al. (2014) describes the original method in complete detail and Lennie et al. (2016) provides an application of the method to an airfoil with microtabs and gurney flaps. In the reformulation described here, the instantaneous damping calculation is applied to the fore-aft motion of the whole rotor, a situation particularly interesting for floating platform wind turbines. It is assumed for this paper that a small pitch angle means that the linear motion will have a greater effect on the wake than the pitching of the rotor plane.

4.1 Cycle Harmonic Damping

Before setting out the derivation of the instantaneous damping coefficient it is first essential to set out the cycle total aerodynamic damping. The approach taken follows the derivation provided by Carta and Niebanck (1967) but for a rotor undergoing fore-aft motion rather than a pitching airfoil section. The authors would like to clearly acknowledge that the following derivation is a modification of existing concepts rather than a completely new derivation.

4.1.1 Linear Harmonic System in a Vacuum

To begin the derivation, let us start with the homogeneous equation of the wind turbine oscillating in linear fore-aft motion(denoted as x).

$$m\ddot{x}^* + c\dot{x}^*(t) + kx^*(t) = 0 \tag{1}$$

where we make an assumption of harmonic motion thus taking;

$$x^*(t) = x_0 e^{i\omega t} \tag{2}$$

which then gives.

$$\dot{x}^*(t) = i\omega x_0 e^{i\omega t} \tag{3}$$

$$\ddot{x}^*(t) = -\omega^2 x_0 e^{i\omega t} \tag{4}$$

Substituting these results into the equation of motion then gives;

$$(-\omega^2 m - \overbrace{i\omega c}^{\mathbb{C}} + k)x^*(t) = 0 \tag{5}$$

As highlighted by Carta and Niebanck (1967), the damping terms are contained within the imaginary term of the equation of motion. They continued that for similar linear systems, the damping should be contained with in the imaginary terms of the differential equation.

4.1.2 Linear Harmonic System in Air

Now introducing the aerodynamic terms into the equation we arrive at the particular equation of

$$(-\omega^2 m - \overbrace{i\omega c}^{\mathbb{C}} + k)x^*(t) = T_U^* \tag{6}$$

Still following the logical steps set down by Carta and Niebanck (1967), the unsteady thrust force can be written as

$$T_U^* = T_1 \ddot{x}^* + T_2^* \dot{x}^* + T_3^* x^* \tag{7}$$

Where,

$$T_2, T_3 \in \mathbb{C} \tag{8}$$

but

$$T_1 \in \mathbb{R} \tag{9}$$

due to the rational that the T_1 represents the apparent mass terms of the system which are identified in terms of the instantaneous reaction forces of an impermeable disk in still air. Instantaneous reaction forces are in phase with the acceleration therefore real. A similar rational was used in the SDOF torsional airfoil oscillator formulation by Carta and Niebanck (1967); Bisplinghoff (2013); Scanlan and Rosenbaum (1951), this time by directly comparing to Theodorsens theory (Theodorsen (1935)) in which a well known distinction is made between the real and imaginary parts of the Bessel function. By substituting in the Cartesian forms of the thrust force;

$$T_2 = T_{2R} + iT_{2I} \tag{10}$$
$$T_3 = T_{3R} + iT_{3I} \tag{11}$$

we arrive at the following equation;

$$(m - T_1)\ddot{x}^* + (c - T_{2R} - iT_{2I})\dot{x}^* + (k - T_{3R} - iM_{3I})x^* = 0 \tag{12}$$

By assuming harmonic motion and collecting real and imaginary terms the equation is reduced to;

$$[(-\omega^2(m - T_1) + \omega T_{2I} + k - T_{3R}) + i(\omega(c - T_{2R}) - T_{3I})]x^* = 0 \tag{13}$$

By eliminating the mechanical damping terms, that is the terms present in a vacuum, the aerodynamic damping can be shown as;

$$\xi = \omega T_{2R} - T_{3I} \tag{14}$$

This result will form a key step in the next decomposition.

4.1.3 Work done by a rotor in fore-aft motion

Let us now take a different decomposition of the thrust force into its constituent steady and unsteady parts. [2]

$$T_{\text{TOTAL}} = T_{\text{MEAN}} + T_{\text{UR}} \cos\omega t + T_{\text{UI}} \sin\omega t \tag{15}$$

Two options exist for the normalization of the thrust force, that is the freestream velocity, or with the inflow velocity thus accounting for the rotor movement. The former assumption simply implies that the unsteady coefficient will contain the freestream effects, for the expected velocity ratios expected for wind turbine pitching movement and freestream velocities. This may cause some peculiarities in the appearance of the data similar that the lift coefficient overshoots seen by Muller-Vahl (2015) and Strangfeld (2015) in unsteady airfoil wind tunnel measurements. Nonetheless, the freestream velocity is taken as convention meaning that the unsteady features will be wrapped up into the unsteady thrust coefficient.

This gives the coefficient form;

$$C_{\text{TTOTAL}} = C_{\text{TMEAN}} + C_{\text{TUR}} + C_{\text{TUI}} \tag{16}$$

The work performed over one cycle of rotor fore and aft motion can be given as;

$$W_T = \oint T_{TOTAL}\mathrm{d}x \tag{17}$$

or in coefficient form,

$$C_{WT} = \oint C_{TTOTAL}\mathrm{d}x \tag{18}$$

Here the differential operator can be switched;

$$\mathrm{d}x = x_0 \sin\omega t\mathrm{d}\omega t \tag{19}$$

and the integral range can be set from $0 < \omega t < -2\pi$ to capture a single cycle finally giving.

$$C_{WT} = -\int_0^{2\pi} [C_{MEAN} + C_{TUR}\cos\omega t + C_{TUI}\sin\omega t]x_0 \sin\omega t\mathrm{d}\omega t \tag{20}$$

By assuming that the thrust force will be simple harmonic(or deviating minimally), evaluating the integral shows that the real unsteady term and the mean terms are both eliminated during the integration leaving

$$C_{WT} = \pi x_0 C_{TUI} \tag{21}$$

This result is the second of the building blocks required to extract the aerodynamic damping from the measurement or simulation data.

---

[2] $T_{Unsteady}$ is hereafter abbreviated to T_U

4.1.4 The third decomposition of the thrust force

Let us now inspect the unsteady thrust force terms further. If we assume the thrust to be a sinusoidal time dependent function, the unsteady thrust force can be given in Cartesian form;

$$T_U = T_{UR} + iT_{UI} \tag{22}$$

For a prescribed motion system the earlier homogeneous equation(equation 13) can be written as a particular equation thus giving;

$$T_U = T_{UR} + iT_{UI} = [(-\omega^2(m - T_1) + \omega T_{2I} + K - T_{3R}) + i(\omega(C - T_{2R}) - T_{3I})]x \tag{23}$$

By equating real and complex terms we get;

$$T_{UI} = [(\omega(C - T_{2R}) - T_{3I})]x \tag{24}$$

This result provides the key to extracting the aerodynamic damping coefficient from the thrust data. From earlier we know that;

$$\xi = (\omega T_{2R} - T_{3I})x \tag{25}$$

These two equations can be related through

$$\xi = -\frac{dT_{UI}}{dx} \tag{26}$$

Or written in the coefficient form

$$\Xi = -\frac{dC_{TUI}}{dx} \tag{27}$$

Using the earlier result of;

$$C_{WT} = \pi x_0 C_{TUI} = x_0 C_0 \sin \phi \tag{28}$$

we can finally arrive at the conclusion that;

$$\Xi_{CYCLE} = \frac{d\frac{C_{WT}}{\pi x_0}}{dx} = -\frac{1}{\pi x_0^2} \oint C_{TTOTAL} dx \tag{29}$$

This equation will form the basis of checking whether the instantaneous equation formulation is correct. In practice it also provides a useful debugging tool for the code implementation.

4.2 Instantaneous damping derivation

In most formulations, certainly as shown above, only a cycle averaged value of aerodynamic damping is found. Bowles, Corke et al. (Bowles et al. (2014); Corke et al. (2014)) provided a breakthrough on this front by using the Hilbert transform to get an

estimate of the magnitude and phase of a signal. If we inspect the following equation from the earlier whole cycle derivation, we may already see the general direction that such a method would follow.

$$C_{WT} = x_0 T_0 \sin \phi \tag{30}$$

The instantaneous damping derivation begins with yet another form of the basic equation of motion for prescribed fore aft motion of a wind turbine rotor.

$$m_t \ddot{x} + h^*(t)\dot{x}(t) + \kappa^* x(t) = T(t) \tag{31}$$

Into which we can insert the apparent mass or inertia of air Pitt and Peters (1983);[3]

$$m_{tair} = \frac{8}{3}\rho R^3 \tag{32}$$

$$I_{tair} = \frac{16}{45}\rho R^5 \tag{33}$$

and then the complex damping and stiffness terms can be described in polar form as;

$$h^* = h_r + ih_I = \bar{h}e^{i\gamma_1} \tag{34}$$

$$\kappa^* = \kappa_r + i\kappa_I = \bar{\kappa}e^{i\gamma_2} \tag{35}$$

Thus we arrive at;

$$\frac{8}{3}\rho R^3 \ddot{x} + \bar{h}e^{i\gamma_1}\dot{x} + \bar{\kappa}e^{i\gamma_2}x = T \tag{36}$$

By introducing the natural frequency parameter ω_0 as;

$$\omega_0 = \sqrt{\frac{3\bar{\kappa}}{8\rho R^3}} \tag{37}$$

the equation reduces to;

$$\ddot{x} + 2h_0\omega_0 e^{i\gamma_1}\dot{x} + \omega_0^2 e^{i\gamma_2}x = \frac{3}{8\rho R^3}T \tag{38}$$

Now taking the Hilbert transform of both sides of the equation.

$$\ddot{\mathcal{X}} + 2h_0\omega_0 e^{i\gamma_1}\dot{\mathcal{X}} + \omega_0^2 e^{i\gamma_2}\mathcal{X} = \frac{3\mathcal{T}}{8\rho R^3} \tag{39}$$

where we replace the thrust and movement with their analytical signal counterparts,

$$\mathcal{X} = X + i\tilde{X} = x_{amp}e^{i\omega t} \tag{40}$$

$$\mathcal{T} = T_u + i\tilde{T}_u = A_t(t)e^{\phi(t)} \tag{41}$$

---

[3]The inertia is not used in this derivation and the apparent mass terms are actually later cancelled out. However it is important to note that the apparent mass analogy can be made for a rotor. If that were not true, then the first term would also be complex and this derivation would be invalidated

Equate the imaginary and real components,

$$-\omega^2 - 2h_0\omega\sin\gamma_1 + \omega_0^2\cos\gamma_2 + i(2h_0\omega\cos\gamma_1 + \omega_0^2\sin\gamma_2) = \frac{3}{8\rho R^3 x_{Amp}}(T_u + i\tilde{T}_u)e^{-i\omega t} \tag{42}$$

Again, the imaginary components correspond to the damping of the system.

$$2h_0\omega\cos\gamma_1 + \omega_0^2\sin\gamma_2 \tag{43}$$

$$= \frac{3}{8\rho R^3 x_{Amp}}(\tilde{T}_u\cos\omega t - T_u\sin\omega t) \tag{44}$$

$$= \frac{3A_T(t)}{8\rho R^3 x_{Amp}}\sin\overbrace{(\phi(t) - \omega t)}^{\psi} \tag{45}$$

The left hand term of this equation correlates to the damping of the system normalized by the apparent mass of the air using a combination of the equations set down by Carta and Niebanck (1967), and the normalization highlighted by Bowles and Corke (Bowles et al. (2014); Corke et al. (2014)).

$$\xi = \frac{A_T(t)}{x_{Amp}}\sin\overbrace{(\phi(t) - \omega t)}^{\psi} \tag{46}$$

Finally we can normalize

$$\Xi(t) = \frac{\xi}{P_{dyn}A} = -\frac{A_{C_t}(t)}{x_{amp}}\sin\psi(t) \tag{47}$$

Where $\tilde{C}_t(t)$ is given by the Hilbert transformed thrust coefficient time series $C_t(t)$;

$$\tilde{C}_t(t) = \mathcal{H}[C_t] = -\frac{1}{\pi}\mathcal{P}\int_{inf}^{inf}\frac{C_t(\tau)}{\tau - t}dt \tag{48}$$

thus giving the analytical signal magnitude;

$$A_{C_t} = \sqrt{C_t^2 + \tilde{C}_t^2} \tag{49}$$

and phase

$$\phi(t) = arg(Y(t)) = arg(C_t + \tilde{C}_t) \tag{50}$$

which gives us the phase difference between the lift and the fore-aft motion

$$\psi(t) = \phi(t) - \omega t \tag{51}$$

from the assumed motion,

$$X(t) = X_0 e^{i\omega t} \tag{52}$$

The time averaged damping then gives us the cycle damping:

$$\Xi_{avg} = -\frac{1}{T}\int_0^T \Xi(t)\mathrm{d}t \qquad (53)$$

Like previously undertaken by Bowles and Corke (Bowles et al. (2014); Corke et al. (2014)) and Lennie et al. (2016) the cycle averaged damping formulation provided by Carta and Niebanck (1967) can be used as a comparison. In this case the comparison will be compared against the formula derived earlier for the fore-aft motion of a rotor.

$$\Xi = \frac{\mathrm{d}\frac{C_{WT}}{\pi X_0}}{\mathrm{d}x} = -\frac{1}{\pi X_0^2}\oint C_{TTOTAL}\mathrm{d}x \qquad (54)$$

Agreement between the two calculations provides a useful (although not completely "leak-proof") verification that the analytical signal is well conditioned and that no implementation errors are present. Verifications undertaken in Lennie et al. (2016) for the original formulation showed less than $< 1\%$ variation between the methods, Bowles et al. (2014) also remarked on the good agreement.

On a practical side, Hilbert transforms are intended to analyse narrowband signals. It was previously established in Lennie et al. (2016), that numerical or experimental noise doesn't cause problems for this formulation - therefore no signal filtering will be applied. Both original and phase averaged data was analysed, although only graphs of the phase averaged data are presented in the paper. In the original time series, stochastic variations due to turbulent inflow are present in cases with turbulence. Otherwise after a few cycles, the results converge to the phase mean.

5   Demonstration Case: Collective Pitch

Having now presented the analysis methods, it is possible to use these methods to investigate an example case of of floating platform wind turbine aeroelasticity. A case was selected that should demonstrate more complicated thrust damping behaviour, the case chosen is harmonic collective pitch in the presence of platform translation. Further potential test cases for future work would include harmonic platform movement in combination;

- yawed inflow

- inflow turbulence

- gusts or sudden changes in direction

- changes in airfoil performance through simulated active flow control

- non-synchronous pitch and platform movements

Harmonic collective pitch in conjunction with platform movement is a complicated test case, but it is still simple enough to give a good demonstration of this particular tool chain. The collective pitch motion was prescribed using the formula

$$\alpha = \alpha_0 \sin(\omega t + \phi_{pitch}) \qquad (55)$$

The test case settings were as follows;

Rotor speed[rpm]	12.1
$\alpha_0[°]$	0.5
ϕ_{pitch} [-]	$0, 0.5\pi, \pi, 1.5\pi$
Inflow velocity [m/s]	11.4
$\omega_{pitch}, \omega_{platform}$[rad/s]	0.5

The collective pitch cycle chosen is not a realistic control regime, it was chosen to give a clear demonstration of the method. The LLFVW simulation was run for 60 seconds with a single cycle chosen for analysis after the initial wake effects had died out. The instantaneous damping was calculated from the thrust data using the method already discussed. As a verification the two cycle average values were compared and had good agreement, the values are presented in table 1.

The cycle averaged aerodynamic damping values do in fact show that collective pitch does have an effect. While thrust damping tends to be positively damped (with this sign convention, that means good damping), we can see that the magnitude of the damping is altered. In figure 7, it is possible to follow the chain of logic that leads to these changes. In the thrust force sequences, it is possible to see that while there are some magnitude shifts, the more important feature is that the phase of the thrust force is shifted. This then manifests as changes to the aerodynamic damping.

A closer inspection reveals an interesting feature, that a 0.5π (green) phase shift of the pitching sequence leads to an almost constant thrust force. This may appear to be favourable to reduce the fatigue loads of the wind turbine. However, what has effectively happened is that there is no force in phase with the velocity of the movement, therefore there is no complex term, thus slightly negative aerodynamic damping. In this case, the system would be relying on the other sources of damping[4] to reduce the amplitude of oscillation.

In the opposite case with a pitch phase shift of 1.5π (yellow), the thrust force is more in phase with the velocity, thus opposing the movement of the rotor is enhanced. The cycle averaged damping reflects this with a stronger damping value. The instantaneous damping value starts to show some departure from a pure harmonic signal. This can be traced to the matching non-linearity in the thrust force which could arise from rotor wake interactions, it is these effects that are difficult to account for in a cycle averaged value. In the literature examples where a pitching airfoil was examined (Bowles et al. (2014); Corke et al. (2014); Lennie et al. (2016)), the non-linearities were very strong due to dynamic stall and caused strong spikes of aerodynamic damping. In simulations where sudden changes of operating conditions are present, the instantaneous damping method will highlight sudden drops in aerodynamic damping when they occur, even if they don't show up in the cycle averaged values.

6 Conclusions

The QBlade implementation of the Free Vortex Lifting Line method(LLFVW) proved to be a useful tool for analysing floating platform wind turbines. Comparisons against two independent test cases, using a variety of methods showed relatively good agreement in thrust forces, rotor power, blade forces and rotor plane induction. Along with the many verifications already

---

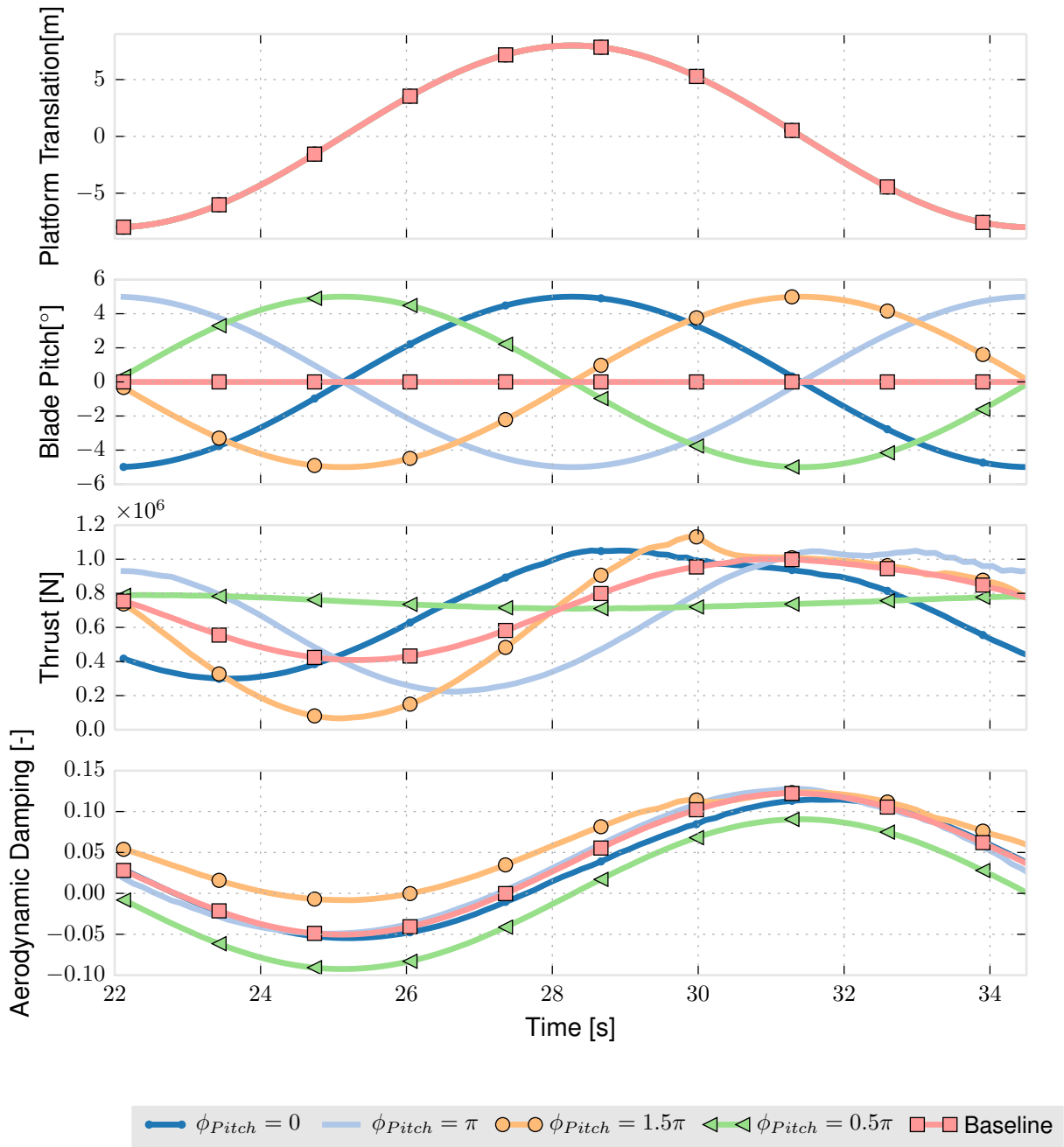[4]i.e. structural or that provided by the floating platform

Figure 7. Collective Pitch Damping Cycles

Table 1. Comparison of Cycle Damping Values

	Averaged Instantaneous Damping	Cycle Averaged Damping	Error
$\phi_{Pitch} = 0$	0.030	0.031	3.5%
$\phi_{Pitch} = \pi$	0.036	0.038	3.5%
$\phi_{Pitch} = 1.5\pi$	0.060	0.062	3.5%
$\phi_{Pitch} = 0.5\pi$	-0.001	-0.001	3.5%
Baseline	0.036	0.037	3.5%

undertaken in literature, it seems that the code will perform solidly even in these challenging cases. Further work is required to extend the same analysis with flexible blades, tower and eventually platform rather than prescribed motion; some of these topics are already under way.

The key results were presented from a new formulation of the instantaneous aerodynamic thrust damping of a wind turbine rotor. A test case showed that the method can help understand aeroelastic stability in complicated cases which may be cyclically damped, but instantaneously unstable. The two different methods of obtaining the cyclic damping agreed giving some confidence in the method.

7 Code availability

The full implementation of QBlade is available for download https://sourceforge.net/projects/qblade/

8 Data availability

No additional data was generated that hasn't been included in this article.

Competing interests. "The authors declare that they have no conflict of interest."

References

T Sebastian and M A Lackner. Characterization of the unsteady aerodynamics of offshore floating wind turbines. (March 2012):339–352, 2013.

David Marten, Matthew Lennie, Georgios Pechlivanoglou, Christian Navid Nayeri, and Christian Oliver Paschereit. Implementation, Optimization, and Validation of a Nonlinear Lifting Line-Free Vortex Wake Module Within the Wind Turbine Simulation Code QBlade. *Journal of Engineering for Gas Turbines and Power*, 138(7):072601, 2015.

Juliane Wendler, David Marten, Christian Navid Nayeri, George Pechlivanoglou, and Christian Oliver Paschereit. GT2016-57184 Implementation and Validation of an Unsteady Aerodynamics Model. In *Proceedings of ASME Turbo Expo 2016: Turbomachinery Technical Conference and Exposition*, pages 1–10, 2016.

Joseph Saverin, David Marten, Georgios Pechlivanoglou, Christian Navid Nayeri, and Christian Oliver Paschereit. GT2016-56290 Coupling of an unsteady lifting line free vortex wake code to the aeroelastic HAWT simulation suite FAST. In *Proceedings of ASME Turbo Expo 2016*, Seoul, South Korea, 2016.

Thanhtoan Tran, Donghyun Kim, and Jinseop Song. Computational Fluid Dynamic Analysis of a Floating Offshore Wind Turbine Experiencing Platform Pitching Motion. *Energies*, 7(8):5011–5026, aug 2014.

Jason M Jonkman. NREL Offshore Baseline 5MW _Onshore with Compiled Controller, 2013.

Patrick O. Bowles, Thomas C. Corke, Dustin G. Coleman, Flint O. Thomas, and Mark Wasikowski. Improved Understanding of Aerodynamic Damping Through the Hilbert Transform. *AIAA Journal*, 52(11):2384–2394, nov 2014.

TC Corke and FO Thomas. Dynamic Stall in Pitching Airfoils: Aerodynamic Damping and Compressibility Effects. *Annual Review of Fluid Mechanics*, 47(1), jan 2015.

Matthew Lennie, Alena Bach, George Pechlivanoglou, Christian Nayeri, and Christian Oliver Paschereit. The Unsteady Aerodynamic Response of an Airfoil with Microtabs and it's Implications for Aerodynamic Damping. *34th Wind Energy Symposium*, (January):1–12, 2016.

M O L Hansen. *Aerodynamics of Wind Turbines*. Earthscan LLC, 2008.

J M Jonkman. Fast Users Guide http://wind.nrel.gov/designcodes/simulators/fast/FAST.pdf.

J B De Vaal, M O L Hansen, and T Moan. Effect of wind turbine surge motion on rotor thrust. (October 2012):105–121, 2014.

D. M. Pitt and D. A. Peters. Rotor Dynamic Inflow Derivatives and Time Constants from Various Inflow Models. In *9th European Rotorcraft Forum*, pages 1–24, 1983.

Franklin O. Carta and Chares F. Niebanck. Prediction of rotor instability at high forward speeds. Technical report, USAAVLABS TR, 1969.

Raymond L Bisplinghoff, Holt Ashley, and Robert L Halfman. *Aeroelasticity*. Courier Corporation, 2013.

Robert H Scanlan and Robert Rosenbaum. *Introduction to the study of aircraft vibration and flutter*. Dover Publications, 1951.

Theodore Theodorsen. General theory of aerodynamic instability and the mechanism of flutter, 1935.

Hanns Friedrich Müller-Vahl. *Wind Turbine Blade Dynamic Stall and its Control*. Doctoral thesis, Technische Universität Berlin, 2015.

Christoph Strangfeld. *Active control of trailing vortices by means of long- and short-wavelength actuation*. Doctor thesis, Technical University of Berlin, 2015.

Eisele, O., Pechlivanoglou, G., Nayeri, C. N., and Paschereit, C. O.: GT2013-94689 The performance of wind turbine airfoils, in: Proceedings of ASME Turbo Expo 2013, pp. 1–10, San Antonio, 2013.

Lennie, M., Pechlivanoglou, G., Marten, D., Nayeri, C. N., and Paschereit, C. O.: GT2015-43249 : A review of wind turbine polar data and it's effect on fatigue loads simulation accuracy, Proceedings of ASME Turbo Expo 2015: Turbine Technical Conference and Exposition GT2015, doi:10.1115/GT2015-43249, 2015.

Christopher L. Rumsey: Turbulence Model Verification and Validation, in: ASME Verification and Validation Symposium, NASA Langley Research Center, Las Vegas, 2016.

Stangfeld, C., Rumsey, C. L., Mueller-Vahl, H., Greenblatt, D., Nayeri, C., and Paschereit, C. O.: Unsteady Thick Airfoil Aerodynamics: Experiments, Computation, and Theory, 45th AIAA Fluid Dynamics Conference, pp. 1–19, doi:10.2514/6.2015-3071, http://arc.aiaa.org/doi/10.2514/6.2015-3071, 2015.